



## NATURAL CONVECTION OF ETHYLENE GLYCOL AND WATER MIXTURE BASED $Al_2O_3$ NANOFLUIDS BETWEEN VERTICAL CONCENTRIC CYLINDERS

Kamil KAHVECİ\* and Elif Büyük ÖĞÜT\*\*

\*Mechanical Engineering Department, Trakya University, 22030 Edirne / Turkey,  
kamilk@trakya.edu.tr, ORCID: 0000-0003-2492-8690

\*\*Vocational School of Hereke Asım Kocabıyık, Kocaeli University, 41800 Hereke-Kocaeli / Turkey,  
elif.ogut@kocaeli.edu.tr, ORCID: 0000-0001-7037-9018

(Geliş Tarihi: 26.12.2019, Kabul Tarihi: 15.05.2020)

**Abstract:** Natural convection of ethylene glycol (EG) and water mixture based  $Al_2O_3$  nanofluids between vertical concentric circular cylinders heated from the inner wall and cooled from the outer wall was investigated numerically in this study. The computations were carried for the Rayleigh numbers of  $10^4$ ,  $10^5$ ,  $10^6$ , and  $10^7$ , nanoparticle volume fractions of 0%, 4% and 8%, ethylene glycol (EG) to water volume ratios of 0:100 %, 50:50%, and 100:0%, the radius ratios of 2, 3 and 4, and aspect ratios of 0.5, 1, and 2. The Brinkman model was used to predict the viscosity and the Yu and Choi model for the thermal conductivity of nanofluid. The results show that the average Nusselt number shows a considerable increase with an increase in the Rayleigh number and radius ratio. The results also show that the average Nusselt number shows a medium increase with increasing nanoparticle volume fraction and a slight increase with increasing volume ratios of EG to water. Furthermore, the results show that the average Nusselt number experiences first an increase then a decrease with an increase in the aspect ratio except for the low Ra numbers. Finally, the average Nusselt number experiences a slight increase with the aspect ratio for the low Rayleigh numbers.

**Keywords:** Natural convection, concentric cylinders, nanofluid,  $Al_2O_3$ , ethylene glycol, water, Rayleigh number, Nusselt number.

### DİK KONSANTRİK SİLİNDİRLER ARASINDAKİ $Al_2O_3$ -ETİLEN GLİKOL VE SU KARIŞIM BAZLI NANOAKIŞKANLARIN DOĞAL KONVEKSİYONU

**Özet:** Bu çalışmada iç duvardan ısıtılan ve dış duvardan soğutulan dikey eş merkezli dairesel silindirler arasında etilen glikol (EG) ve su karışım bazlı  $Al_2O_3$  nanoakışkanların doğal konveksiyonu sayısal olarak incelenmiştir. Hesaplamalarda Rayleigh sayıları  $10^4$ ,  $10^5$ ,  $10^6$  ve  $10^7$ , nanoparçacık hacim fraksiyonları % 0, % 4 ve % 8, etilen glikol (EG) - su hacim oranları %0:100, % 50:50 ve % 100: 0, yarıçap oranları 2, 3 ve 4 ve görünüş oranları 0.5, 1 ve 2 olarak alınmıştır. Nanoakışkanın termal iletkenliği için Yu ve Choi modeli ve viskozitesi içinde Brinkman modeli kullanılmıştır. Sonuçlar, ortalama Nusselt sayısının Rayleigh sayısı ve yarıçap oranındaki artışla önemli miktarlarda arttığını göstermektedir. Sonuçlar ayrıca ortalama Nusselt sayısının artan nanoparçacık hacim fraksiyonu ile orta seviyede bir artış ve EG-su hacim oranı artışı ile küçük bir artış sergilediğini göstermektedir. Sonuçlar ayrıca, ortalama Nusselt sayısının düşük Ra sayıları dışında, görünüş oranındaki artışla önce artmakta sonra bir azalma göstermektedir. Son olarak, ortalama Nusselt sayısı düşük Rayleigh sayıları için artan görünüş oranıyla küçük bir artış göstermektedir.

**Anahtar Kelimeler:** Doğal konveksiyon, konsentrik silindirler, nanoakışkan,  $Al_2O_3$ , etilen glikol, su, Rayleigh sayısı, Nusselt sayısı.

#### NOMENCLATURE

|       |   |                      |  |
|-------|---|----------------------|--|
| A     | aspect ratio  | $R_o$                | outer radius of the annulus (m)            |
| $c_p$ | specific heat at constant pressure ( $J kg^{-1} K^{-1}$ ) | T                    | temperature ( $^{\circ}C$ )                |
| g     | acceleration due to gravity ( $m s^{-2}$ )                | $v_r$                | velocity in the r-direction ( $m s^{-1}$ ) |
| k     | thermal conductivity ( $W m^{-1} K^{-1}$ )                | $v_z$                | velocity in the z-direction ( $m s^{-1}$ ) |
| H     | height (m)  | r                    | coordinate in the radial direction (m)     |
| Nu    | Nusselt number  | z                    | coordinate in the axial direction (m)      |
| P     | pressure ( $kg m^{-1} s^{-2}$ )                           | <i>Greek symbols</i> |  |
| Pr    | Prandtl number  | $\alpha$             | thermal diffusivity ( $m^2 s^{-1}$ )       |
| Ra    | Rayleigh number   | $\beta$              | thermal expansion coefficient ( $K^{-1}$ ) |
| $R_i$ | inner radius of the annulus (m)                           | $\phi$               | solid volume fraction                      |
|       |   | $\mu$                | dynamic viscosity ( $kg m^{-1} s^{-1}$ )   |
|       |   | $\nu$                | kinematic viscosity ( $m^2 s^{-1}$ )       |

|                     |                               |
|---------------------|-------------------------------|
| $\rho$              | density (kg m <sup>-3</sup> ) |
| <i>Subscripts</i>   |                               |
| C                   | cold                          |
| f                   | fluid                         |
| H                   | hot                           |
| nf                  | nanofluid                     |
| s                   | solid                         |
| <i>Superscripts</i> |                               |
| *                   | dimensional variable          |

## INTRODUCTION

Natural convection in cavities has been the focus of interest owing to engineering applications such as energy transfer in buildings, heat exchangers, thermal storage systems, cooling of electronic components and solar collectors. One of the primary limitations in the thermal performance of cavities is the low thermal conductivity of conventional fluids. This limitation has been overcome by the addition of nano-sized solid particles with high thermal conductivity to base fluid. The term nanofluid is used to designate this type of mixtures. Keblinski *et al.* (2002) discussed four different mechanisms for heat transfer enhancement potential of nanofluids: Brownian motion, solid-like liquid layering, the nature of heat transfer, and clustering. They concluded that liquid layering is the most important mechanism for the increase in thermal conductivity.

There are many studies in the literature looking into the effects of nanoparticle usage on natural, forced and mixed convection heat transfer. However, the studies in the literature are mostly for rectangular enclosures. There are also some studies for other geometries such as cylinders. Cianfrini *et al.* (2011) investigated theoretically natural convection of nanofluids between horizontal concentric cylinders. The results show that heat transfer increases with increasing nanoparticle volume fraction up to an optimal volume fraction and excessive increase in the volume fraction may bring to remarkable deteriorations in thermal performance with respect to the reference pure base liquid. Abu-Nada *et al.* (2008) studied the natural convection of nanofluids in horizontal concentric annuli numerically. The results show that the nano-sized solid particles with high thermal conductivities result in a substantial enhancement in heat transfer for the high Ra numbers and high L/D ratio. On the other hand, the nano-sized solid particles with low thermal conductivities cause a reduction in heat transfer for the modest Ra numbers. Yu *et al.* (2012) conducted a numerical study of transient natural convection heat transfer of aqueous nanofluids in a horizontal concentric annulus and observed that the average Nu number takes gradually lower values with increasing nanoparticle volume fraction. Selimefendigil and Öztop (2017) examined magneto-hydrodynamic natural convection of nanofluids in a partitioned horizontal annulus numerically and observed that the average Nu number increases as the partition thickness and the Ra number increase and the Hartmann number decreases. They also

observed that the effect of the partition thickness is more noticeable in the conduction dominant regime when the Ra number is low and the Ha number is high. Haq *et al.* (2017) studied the magneto-hydrodynamic flow of engine oil based carbon nanotubes between two concentric cylinders. The results show that the maximum value of velocity decreases through the increase in the carbon nanotube volume fraction. The results also show that the addition of carbon nanotubes tremendously increases the temperature of the base fluid. Increasing the Hartmann number leads to an increase in the velocity of nanofluid in the middle of the channel. Hajimohammadi (2017) conducted a theoretical study on flow and heat transfer characteristics of metallic nanofluids in a cylindrical domain by single-phase and two-phase models. The results show that the influence of nano-sized solid particles on the shear stress and heat transfer augmentation attained by a single-phase model are higher up to 3% as compared to those of the two-phase model. Turkyilmazoglu (2015) investigated convective heat transfer of nanofluids in circular concentric cylinders under the influence of partial velocity slips on the surfaces and concluded that the velocity slip causes a substantial increase in heat transfer and its effect is more noticeable when the nanoparticles are added into the pure water. Togun *et al.* (2016) performed a numerical simulation on flow and heat transfer of Al<sub>2</sub>O<sub>3</sub> based nanofluid in co-axial cylinders having a sudden expansion. Their results show that the separation areas formed after the sudden expansions affect the heat transfer substantially. Alawi *et al.* (2014) studied natural convection heat transfer of nanofluids in a horizontal concentric annulus between the outer cylinder and inner flat-tube numerically and found that the average Nusselt number increases with the hydraulic radius ratio, orientation angles, and Rayleigh number. Maghlany and Elazm (2016) conducted a numerical investigation on mixed convection in an eccentric horizontal annulus with a rotating inner cylinder and concluded that the nanoparticle addition increases heat transfer at mixed or natural convection dominant regime and it has an opposite effect at forced convection dominant regime. Dawood *et al.* (2017) performed a numerical study on the mixed convection of several nanofluids in an elliptic annulus. The results indicate that the SiO<sub>2</sub>-EG nanofluid yields the highest Nu number. The Nu number increases as the nanoparticle fraction and the Re number get higher values; however, it decreases as the nanoparticle diameter increases. Sasmal (2017) simulated nanofluid flow and heat transfer from an elliptic cylinder. The results indicate that the average Nu number for CuO nanofluids with a higher diameter increases with the increasing nanoparticle volume fraction without depending on the values of cylinder axis ratio and the Reynolds number, whereas for CuO nanofluids with a lower diameter, there is an optimum value of solid volume fraction and the Nu number starts to decline with the further addition of nanoparticles. Özdemir and Ögüt (2019) studied fully developed turbulent flow between horizontal concentric pipes and concluded that the Nusselt number increases

with increasing Re number and ethylene glycol concentration and decreases with an increase in the radius ratio and inlet temperature. They also found that the pumping power shows an increase with the Re number, ethylene glycol concentration, nanoparticle volume fraction and radius ratio and decreases with the inlet temperature.

All aforementioned studies are on convective heat transfer between horizontal concentric cylinders. There are also few studies on convective heat transfer between vertical cylinders. Öztuna *et al.* (2011) simulated natural convection heat transfer of water-based CuO nanofluid between vertical concentric cylinders for a fixed height and outer diameter and concluded that the heat transfer shows a substantial increase as the solid volume fraction and Ra number increase. Srinivasacharya and Shafeurrahman (2017) studied magneto-hydrodynamic mixed convection flow of nanofluid between two vertical concentric cylinders and found that when the Ha number increases, the temperature attains higher values, whereas velocity decreases. Wu *et al.* (2017) investigated mixed convection of a dense suspension between two vertical cylinders and concluded that the temperature difference between the inner and the outer cylinders creates a layer of low particle concentration near the inner cylinder. Chen *et al.* (2016) performed numerical simulations on the forced convection of a nanofluid in the gap between concentric cylinders with a rotational spindle. The results indicate that the heat flux increases 23% for the volume fraction of 10% and 20% when the angular velocity of the spindle is changed from 5 rad/s to 25 rad/s.

A single fluid such as water, ethylene glycol, and propylene glycol are usually used as a base fluid in a nanofluid- mixture. However, the use of two-fluid mixtures as a base fluid has some advantages over a single fluid. For instance, two-fluid mixtures consisting of water and glycol has a higher thermal conductivity than pure glycol and a lower freezing temperature than water (Cabaleiro *et al.*, 2015). Therefore, glycol and water mixture is a good alternative for some practical applications such as antifreeze in vehicle engines or transfer medium in solar heating systems (Heris *et al.*, 2014; Said *et al.* 2013).

From the literature given above, it can be seen that the natural convection of nanofluid between vertical concentric cylinders has not been studied for a wide range of geometric parameters and base fluid of two-fluid mixtures. In addition, the present study assumes Al<sub>2</sub>O<sub>3</sub> nanoparticle that exhibits several excellent properties such as very good stability and chemical inertness (Hinge *et al.*, 2017).

In accordance with the previous discussion, natural convection of EG and water mixture based nanofluids between vertical concentric cylinders was investigated in this study for a wide range of geometric and transport parameters.

## ANALYSIS

The geometry and coordinate system are given in Fig. 1. The height of the vertical cylinders is H and it was assumed constant. R<sub>i</sub> is the radius of the inner cylinder and R<sub>o</sub> is the radius of the outer cylinder. The nanofluid between the cylinders is heated and cooled by the vertical walls. The horizontal walls are assumed to be adiabatic. The nanofluid was assumed as an incompressible Newtonian fluid, and flow was assumed laminar. A single-phase approach was used to model the fluid flow and heat transfer. As a result, the fluid particles and nanoparticles were assumed to be in thermal equilibrium and they flow at the same velocity. The thermophysical properties were taken constant except for density in the buoyancy force term. The thermal radiation and viscous dissipation were assumed to be negligible.

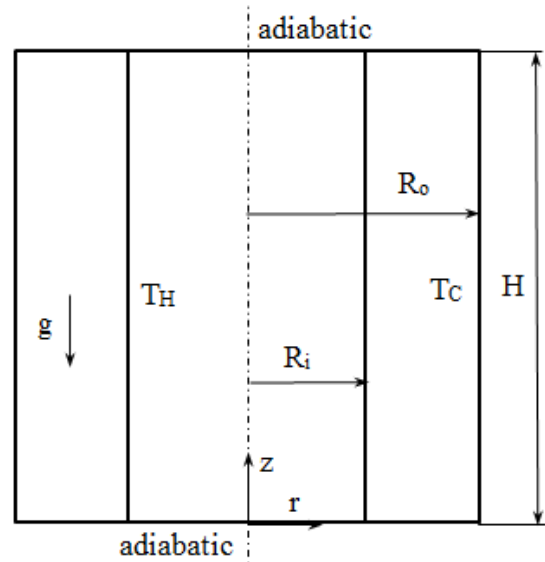


Figure 1. Geometry and the coordinate system.

The dimensionless variables used in the study are given below:

$$r = \frac{x^*}{R}, z = \frac{y^*}{R}, v_r = \frac{v_r^*}{\alpha_f R}, v_z = \frac{v_z^*}{\alpha_f R}, P = \frac{R^2}{\rho_{f,0} \alpha_f^2} P^*,$$

$$T = \frac{T^* - T_C^*}{T_H^* - T_C^*}, A = \frac{H}{R} \quad (1)$$

where  $v_r^*$ ,  $v_z^*$  are the dimensional velocities in the  $r^*$  and  $z^*$  directions,  $p^*$  and  $T^*$  are the dimensional pressure and temperature,  $\rho_{f,0}$  is the density of the fluid at  $T_C$ , and  $\alpha$  is the thermal diffusivity.  $R_i$  and  $R_o$  are the inner and outer radii of the annulus, and  $H$  is its height;  $R = R_o - R_i$ .

The nondimensional governing equations can be expressed as:

$$\frac{\partial v_r}{\partial r} + \frac{v_r}{r} + \frac{\partial v_z}{\partial z} = 0 \quad (2)$$

$$v_r \frac{\partial v_r}{\partial r} + v_z \frac{\partial v_r}{\partial z} = -\frac{\rho_f}{\rho_{nf}} \frac{\partial P}{\partial r} +$$

$$\frac{v_{nf}}{v_f} Pr \left( \frac{\partial^2 v_r}{\partial r^2} + \frac{1}{r} \frac{\partial v_r}{\partial r} + \frac{\partial^2 v_r}{\partial z^2} - \frac{v_r}{r^2} \right) \quad (3)$$

$$v_r \frac{\partial v_z}{\partial r} + v_z \frac{\partial v_z}{\partial z} = - \frac{\rho_f}{\rho_{nf}} \frac{\partial P}{\partial z} + \frac{v_{nf}}{v_f} Pr \left( \frac{\partial^2 v_z}{\partial r^2} + \frac{1}{r} \frac{\partial v_z}{\partial r} + \frac{\partial^2 v_z}{\partial z^2} \right) + \frac{(\rho\beta)_{nf}}{\rho_{nf}\beta_f} Ra Pr T \quad (4)$$

$$v_r \frac{\partial T}{\partial r} + v_z \frac{\partial T}{\partial z} = \frac{\alpha_{nf}}{\alpha_f} \left( \frac{\partial^2 T}{\partial r^2} + \frac{1}{r} \frac{\partial T}{\partial r} + \frac{\partial^2 T}{\partial z^2} \right) \quad (5)$$

here  $\nu$  is the kinematic viscosity of the fluid and  $\beta$  is the coefficient of thermal expansion. The Pr and Ra numbers are defined as:

$$Pr = \frac{\nu_f}{\alpha_f}, \quad Ra = \frac{g\beta_f R^3 \Delta T^*}{\nu_f \alpha_f} \quad (6)$$

where  $g$  is the gravitational acceleration and  $\Delta T^*$  is the temperature difference.

The boundary conditions of the non-dimensional equations can be expressed as:

$$v_r|_s = 0, \quad v_z|_s = 0 \quad (7)$$

$$T|_{r=R_0} = 0 \quad (8)$$

$$T|_{r=R_i} = 1 \quad (9)$$

$$\frac{\partial T}{\partial z} \Big|_{z=0} = 0, \quad \frac{\partial T}{\partial z} \Big|_{z=H} = 0 \quad (10)$$

The nanofluid viscosity is mostly predicted using the Brinkman (1952) model. This viscosity model given below was also used in this study:

$$\mu_{nf} = \frac{\mu_f}{(1-\phi)^{2.5}} \quad (11)$$

where  $\phi$  is the solid volume fraction. The nanofluid thermal conductivity was predicted by the Yu and Choi (2003) model, which takes into account the effect of liquid layering on nanoparticles:

$$\frac{k_{nf}}{k_f} = \frac{k_s + 2k_f + 2(k_s - k_f)(1+\eta)^3 \phi}{k_s + 2k_f - (k_s - k_f)(1+\eta)^3 \phi} \quad (12)$$

where  $\eta$  is the ratio of the thickness of liquid layering to the radius of a nanoparticle.

The other thermophysical properties of nanofluid were expressed using the following relations (Xuan and Roetzel, 2000):

$$\rho_{nf,o} = (1-\phi)\rho_{f,o} + \phi\rho_{s,o} \quad (13)$$

$$(\rho c_p)_{nf} = (1-\phi)\rho_f c_{pf} + \phi\rho_s c_{ps} \quad (14)$$

$$(\rho\beta)_{nf} = (1-\phi)\rho_f \beta_f + \phi\rho_s \beta_s \quad (15)$$

The subscripts f, nf, and s represent the base fluid, nanofluid and solid.

The local and average Nu numbers on the hot inner wall were expressed as follows:

$$Nu = - \frac{k_{eff}}{k_f} \frac{\partial T}{\partial r} \Big|_{r=R_i} \quad (16)$$

$$Nu_a = - \frac{1}{A} \frac{k_{eff}}{k_f} \int_0^A \frac{\partial T}{\partial r} \Big|_{r=R_i} dz \quad (17)$$

## RESULTS AND DISCUSSION

The computational results were obtained by a finite element simulation software (Comsol Multiphysics) for the Ra numbers of  $10^4$  to  $10^7$ , for three different solid volume fractions, 0%, 4%, and 8%, for three different volume ratios of EG to water, 0:100%, 50:50%, 100:0 %, for the aspect ratios of 0.5, 1, and 2, and the radius ratios of 2, 3, and 4. The finite element method was used as it generally has higher accuracy (Jiajan, 2010; Fuchs and Eguchi, 1988). The volumetric volume fraction was limited to 8% as the Brinkman (1952) viscosity model used in this study assumes that any flow disturbance around one particle does not have interaction with that of another and this interaction can not be ignored for the concentrations  $>10\%$  (Mitra and Chakraborty, 2011).  $Al_2O_3$  was selected as the nanoparticle and the ratio of the liquid layering thickness to the radius of a nanoparticle ( $\eta$ ) was taken fixed at 0.1. This value of  $\eta$  yields a good agreement between model predictions and experimental results. The thermophysical properties of the fluids and  $Al_2O_3$  nanoparticle are seen in Table 1.  $err \leq 10^{-6}$  is chosen as convergence criteria for the governing variables in the study, where  $err$  is the relative error in the Euclidean norm defined as:

$$err = \sqrt{\frac{1}{N} \sum_{i=1}^N \left( \frac{|E_i|}{W_i} \right)^2} \Bigg|^{1/2}, \quad W_i = \max(|U_i|, |S_i|) \quad (18)$$

where  $E_i$  the error,  $U_i$  the dependent variable, and  $S$  the scale factor.

Prior to the validation of the results, a study on the mesh-dependency was carried out. As can be observed from Table 2, the results of the average Nu number are mesh-independent up to three figures after the decimal point for the max element size of 0.05 in the computational domain. Therefore, all computational results were obtained for the aforementioned mesh size.

**Table 1.** Thermophysical properties.

| Property                                    | 0:100%<br>EG/W | 50:50%<br>EG/W | 100:0%<br>EG/W | Al <sub>2</sub> O <sub>3</sub> |
|---|----------------|----------------|----------------|--------------------------------|
| $\rho$ (kg/m <sup>3</sup> )                 | 997.1          | 1071.1         | 1132           | 3970                           |
| $c_p$ (j/kg K)                              | 4180           | 3300           | 2349           | 765                            |
| $k$ (W/m K)                                 | 0.613          | 0.37           | 0.258          | 40                             |
| $\mu$ (mPa/s)                               | 0.891          | 3.39           | 15.1           | -                              |
| $\alpha \times 10^7$<br>(m <sup>2</sup> /s) | 1.47           | 1.046          | 0.97           | 131.7                          |
| $\beta$ (K <sup>-1</sup> )                  | 0.00021        | 0.00039        | 0.00057        | 0.000024                       |
| Pr  | 6.07           | 30.235         | 137.48         | -                              |

The results of the numerical model were validated by comparing the results for the Pr=1 with the results of Davis and Thomas (1969), which was obtained by a finite difference method. The comparison seen in Table 3 shows that there is a good agreement between these two results. The difference between the results can be attributed to the relatively coarse mesh used in the study of Davis and Thomas (1969).

**Table 2.** Mesh dependency for A=1,  $\phi=0.08$  and 50:50 EG/W.

| Ra              | Max Element size | The number of elements | Nu <sub>a</sub> |
|-----------------|------------------|------------------------|-----------------|
| 10 <sup>4</sup> | 0.07             | 77504                  | 3.503           |
|                 | 0.06             | 77682                  | 3.502           |
|                 | 0.05             | 77678                  | 3.502           |
|                 | 0.04             | 77752                  | 3.502           |
| 10 <sup>5</sup> | 0.07             | 77504                  | 7.251           |
|                 | 0.06             | 77682                  | 7.252           |
|                 | 0.05             | 77678                  | 7.251           |
|                 | 0.04             | 77752                  | 7.252           |
| 10 <sup>6</sup> | 0.07             | 77504                  | 14.186          |
|                 | 0.06             | 77682                  | 14.185          |
|                 | 0.05             | 77678                  | 14.188          |
|                 | 0.04             | 77752                  | 14.188          |
| 10 <sup>7</sup> | 0.07             | 77504                  | 26.706          |
|                 | 0.06             | 77682                  | 26.705          |
|                 | 0.05             | 77678                  | 26.705          |
|                 | 0.04             | 77752                  | 26.704          |

**Table 3.** Validation of the numerical results.

| Ro/Ri | A  | Davis and Thomas [29] | Nu <sub>a</sub> |
|-------|----|-----------------------|-----------------|
| 2     | 5  | 5.67                  | 5.05            |
|       | 10 | 4.63                  | 4.40            |
| 3     | 5  | 6.44                  | 5.83            |
|       | 10 | 5.27                  | 5.11            |
| 4     | 5  | 6.79                  | 6.43            |
|       | 10 | 5.77                  | 5.62            |

The flow and heat transfer between the concentric cylinders were represented by streamlines and isotherms for various values of the governing parameters. The streamlines and isotherms were only given for water-based nanofluid as the forms of streamlines and isotherms are very similar for other base fluids considered in this study. The streamlines (on the left) and isotherms (on the right) between the

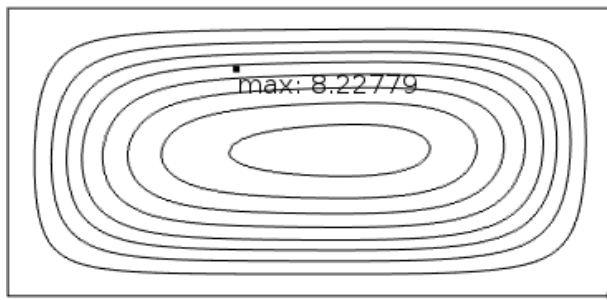
concentric cylinders are seen in Figure 2 for the aspect ratio of A=0.5. As can be seen that there is a unicellular flow in the flow domain for all Rayleigh numbers. The heat transfer for the low Rayleigh numbers is conduction dominant. This is as a result of the nearly parallel isotherms to the vertical walls. The heated wall is shorter than the unheated wall that contributes viscous forces and weakens convection currents. That is the main reason for the conduction dominant heat transfer. As can be observed, convection strengthens with increasing Ra number and the flow regime evolves to the boundary flow regime along the heated and hot and cold wall. This is deduced from the increasing steepness of isotherms near the hot and cold walls and plateau formation in the core region of the cylindrical annulus. The circulation center is shifted rightward with increasing Ra number. As can be seen from Figure 2 that nanoparticle usage causes a decrease in the convection intensity. This is a result of an increase in the viscosity of the fluid with the addition of solid nanoparticles to the base fluid. The nanoparticle addition to the base fluid results in an increase in energy transport from the hot wall to the fluid particles due to the increase in the fluid thermal conductivity. As a result, isotherms along the hot wall near the bottom wall move away from the hot wall, isotherms along the hot wall near the top wall get closer to the hot wall. The streamlines and isotherms between the concentric cylinders are seen in Figures 3 and 4 for the aspect ratios of A=1 and 2. As can be seen, circulation intensity shows an increase with the aspect ratio depending on the positive influence of the bigger hot surface on heat transfer. A decrease in circulation intensity with nanoparticle addition is not seen for these aspect ratios as a result of compensation of the positive influence of thermal conductivity increase on the circulation strength. As can be seen from Figure 3 that the flow becomes multicellular in the core region for the high values of the Rayleigh number for A=1. The elliptic circulation cells become rectangular with an increase in the Rayleigh number as a result of strengthening circulation and the restriction of vertical and horizontal walls on the flow.

The variation of the local Nu number on the hot inner wall is seen in Figure 5 for various values of the Ra number, nanoparticle volume fraction and aspect ratio. The local Nusselt number first shows an increase and gets its maximum value along the hot inner wall of the cylinder. Then it shows first a fast decrease and then almost a linear decrease. As it is approached the top wall, the decrease in the local Nusselt number shows an increase. The boundary layer is thinner and therefore temperature gradient is higher near the bottom wall. However, viscous forces are also higher near the bottom wall. This has a negative influence on the temperature gradient and therefore the local Nu number takes its highest value at a certain distance from the bottom wall. The local Nu number shows a faster decrease near the top wall due to the limitation of the top wall on the movement of fluid particles and higher viscous forces near this wall. As can be observed from Figure 5a, the

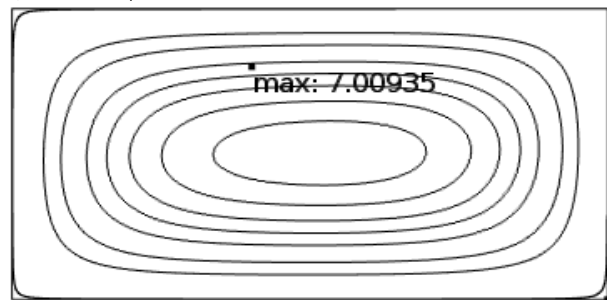
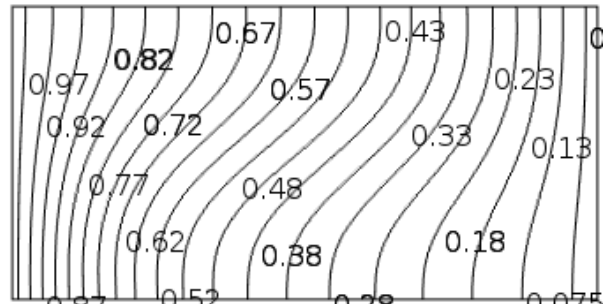
local Nu number almost remains constant for the low values of the Ra number. This justifies the conduction dominant heat transfer deduced previously from isotherms. It can also be observed that the local Nu number shows a significant increase with increasing Ra number depending on strengthening convection. The addition of nanoparticles also results in an increase in the local Nu number as a result of the positive effect of higher thermal conductivity. The local Nu number shows first an increase then a decrease with increasing aspect ratio. The increase can be ascribed to the higher hot surface area and the relative decrease in the viscous forces. The decrease can be attributed to the significant decrease in heat transfer in the upper part of the annulus due to the decrease in the temperature gradient between the hot wall and heated fluid particles along the hot wall.

The average Nu number is given in Tables 4-6 for various values of solid volume fraction, Ra number, volume ratios of EG to water, and aspect ratio. As can be observed from Tables 4-6 that the most effective parameter on the average Nu number is Ra number and its increase causes high increases in the average heat transfer rate depending on the strengthening

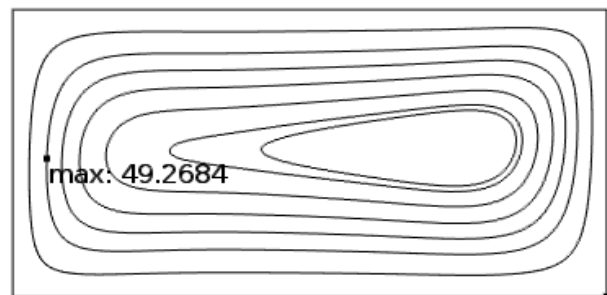
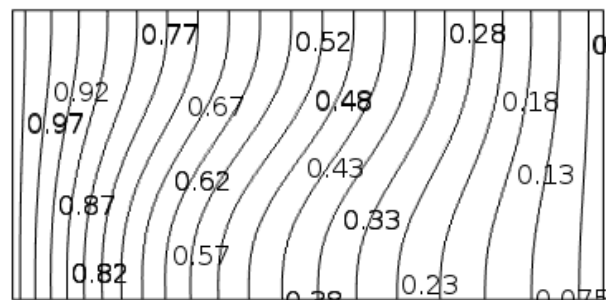
convection. The average Nu number also experiences a substantial increase with the nanoparticle addition. As can also be observed from Tables 4-6 increasing the volume ratio of EG to water also causes a slight increase in the average Nu number depending on the increase in the Prandtl number. The increase remains limited as increasing the ratio of ethylene glycol to water also causes a significant increase in the viscosity and therefore a decrease in the flow strength. Increase in the average Nu number with volume fraction of ethylene glycol to water ratio takes higher values when the Ra number increases. As can be observed from Tables 4-6 that the average Nu number experiences first an increase and then a decrease with increasing aspect ratio for the high values of the Ra number. The average Nu number shows a steady increase with the aspect ratio for the low Ra numbers. The variation of the average Nu number with radius ratio is given in Tables 7-9. The radius ratio is also a significant factor and the heat transfer experiences a considerable increase with increasing radius ratio. The influence of the radius ratio increases slightly with increasing solid volume fraction. Increasing radius ratio leads to a higher increase in the heat transfer for the low Ra numbers and the high values of the solid volume fraction.



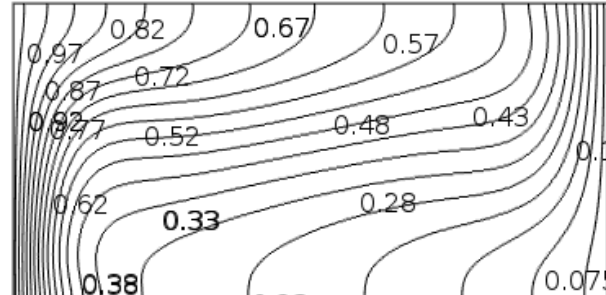
a)  $Ra=10^4$ ,  $\phi=0.0$



b)  $Ra=10^4$ ,  $\phi=0.08$



c)  $Ra=10^5$ ,  $\phi=0.0$



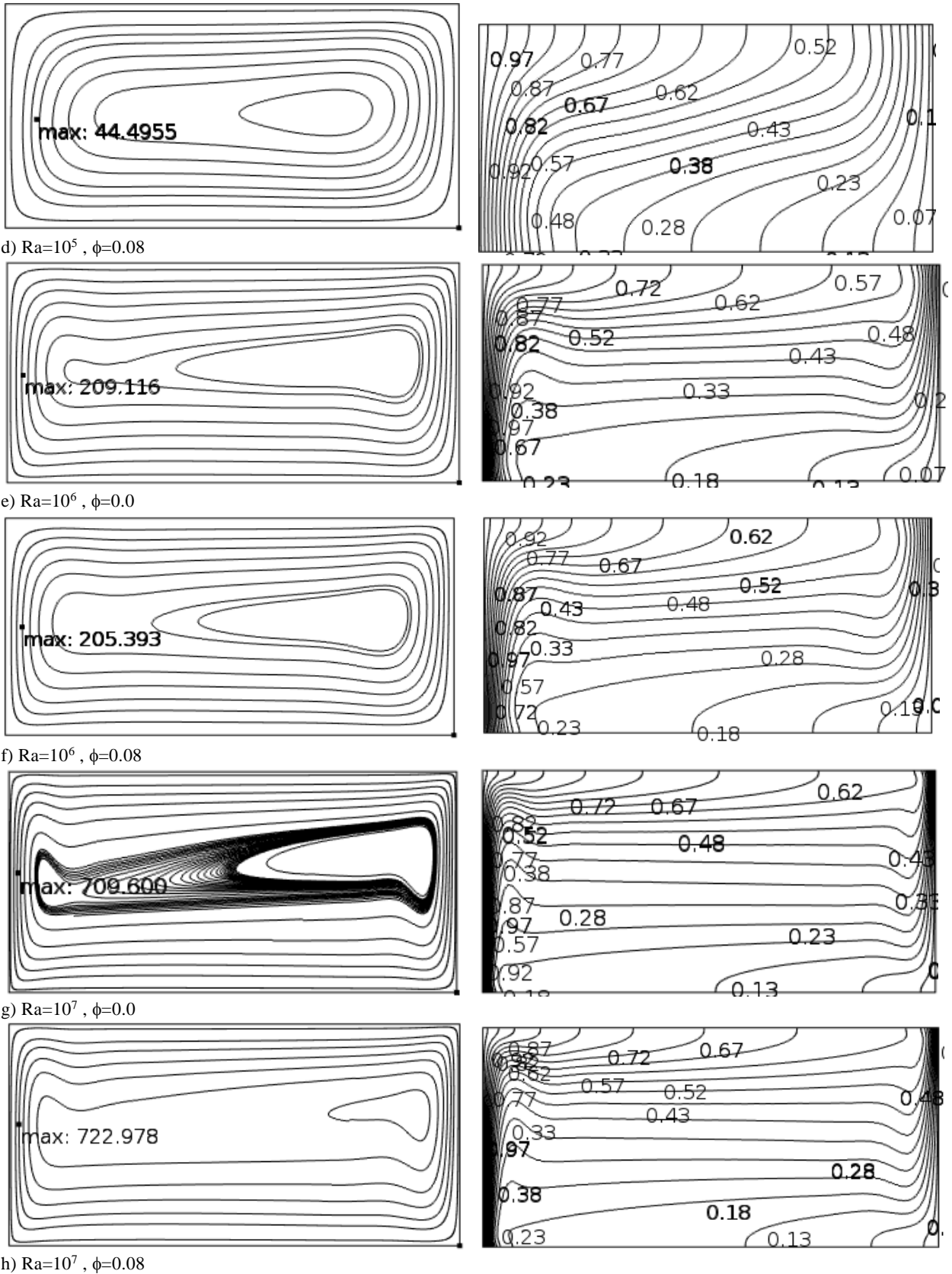


**Figure 2.** Streamlines (on the left) and isotherms (on the right) for 0:100% EG/W-based nanofluid for  $A=0.5$  and  $R_0/R_i=2$ .

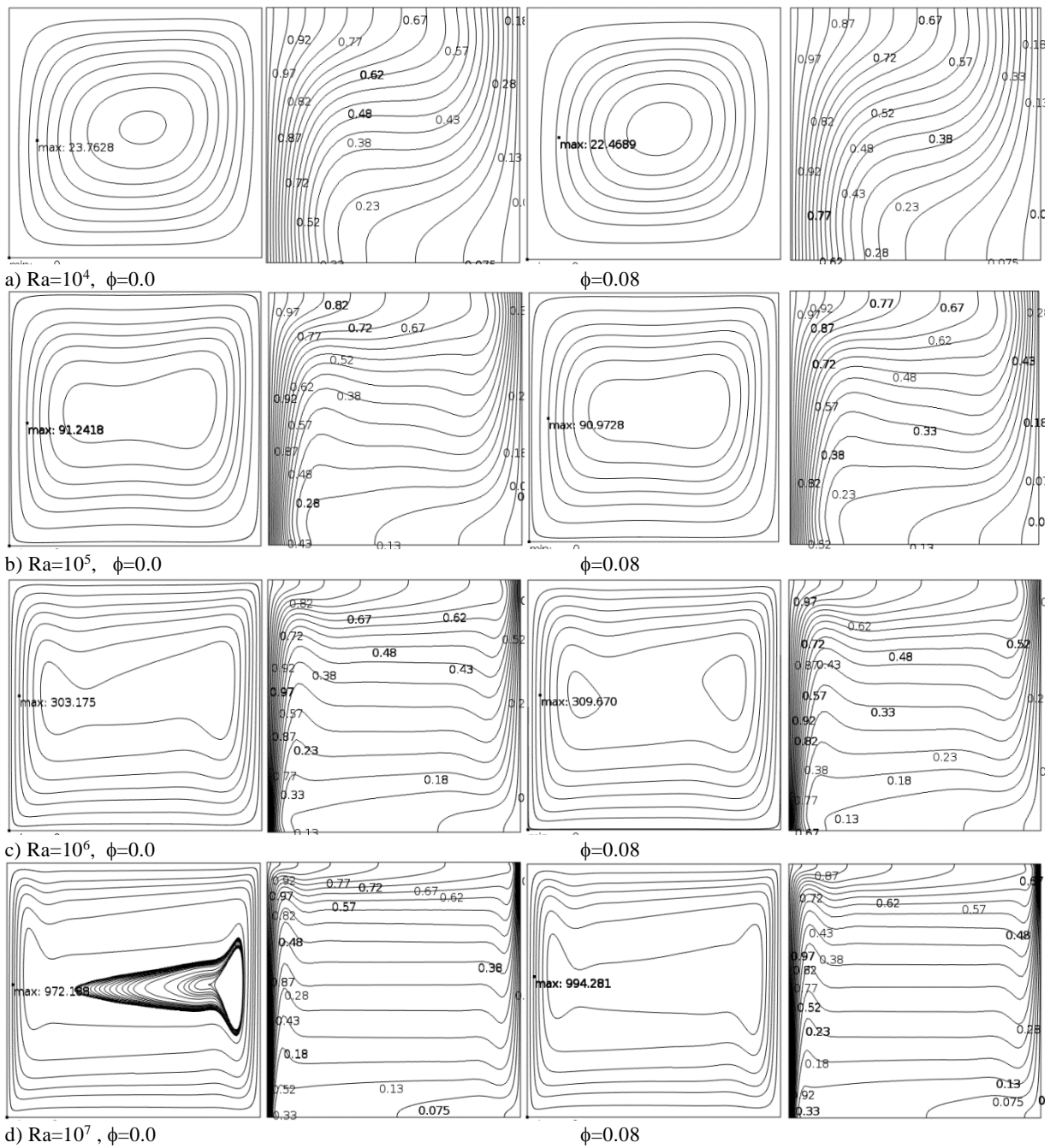
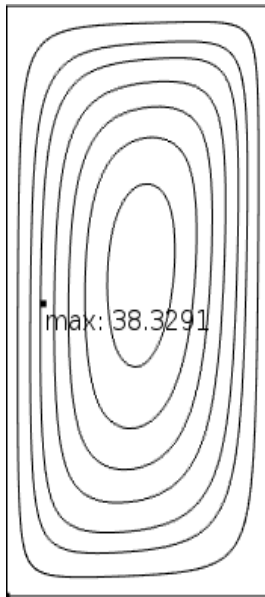
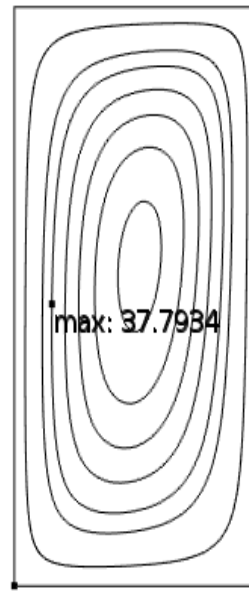
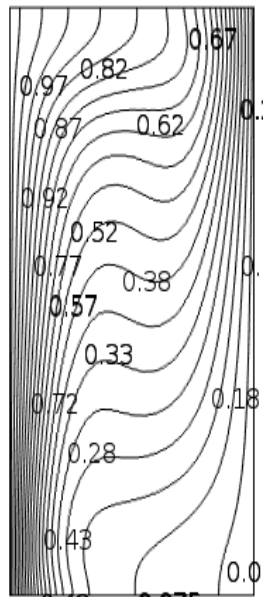


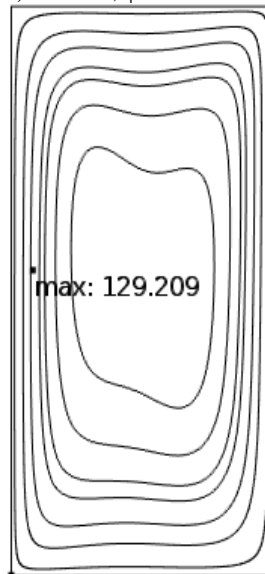
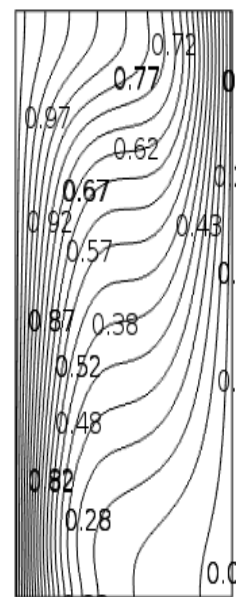
**Figure 3.** Streamlines (on the left) and isotherms (on the right) for 0:100% EG/W-based nanofluid for  $A=1$  and  $R_o/R_i=2$ .



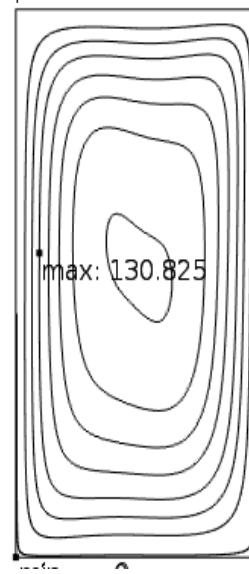
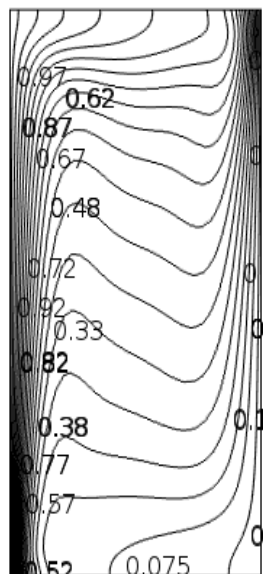
a)  $Ra=10^4$ ,  $\phi=0.0$



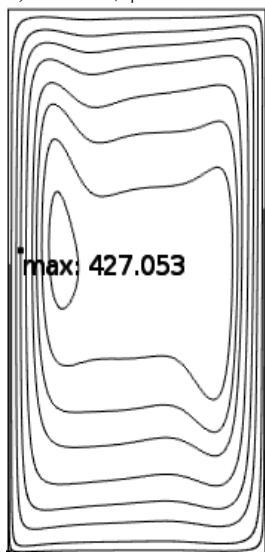
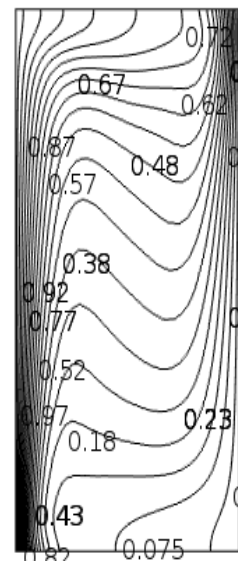
$\phi=0.08$



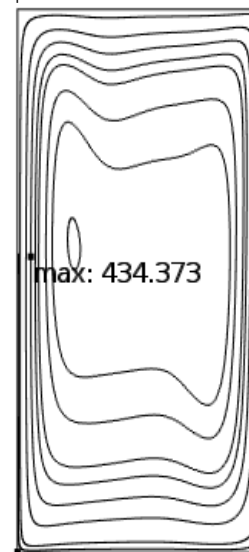
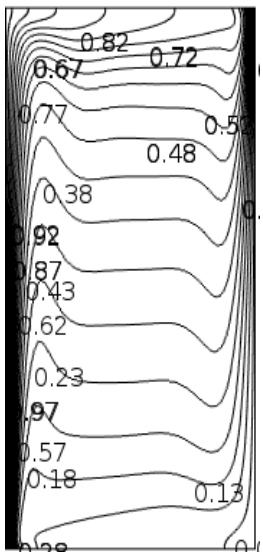
b)  $Ra=10^5$ ,  $\phi=0.0$



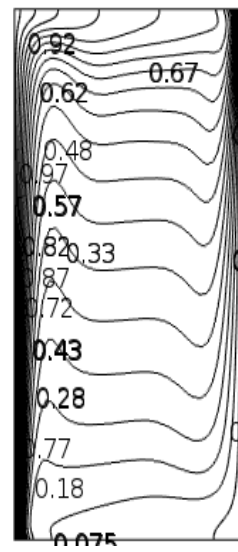
$\phi=0.08$

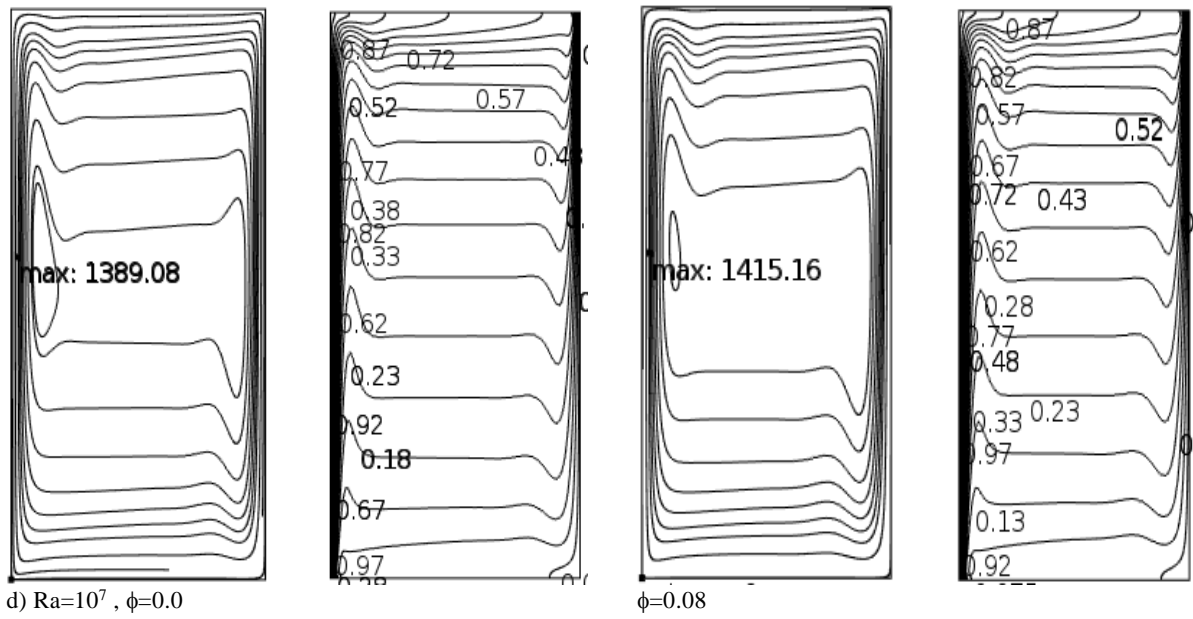


c)  $Ra=10^6$ ,  $\phi=0.0$

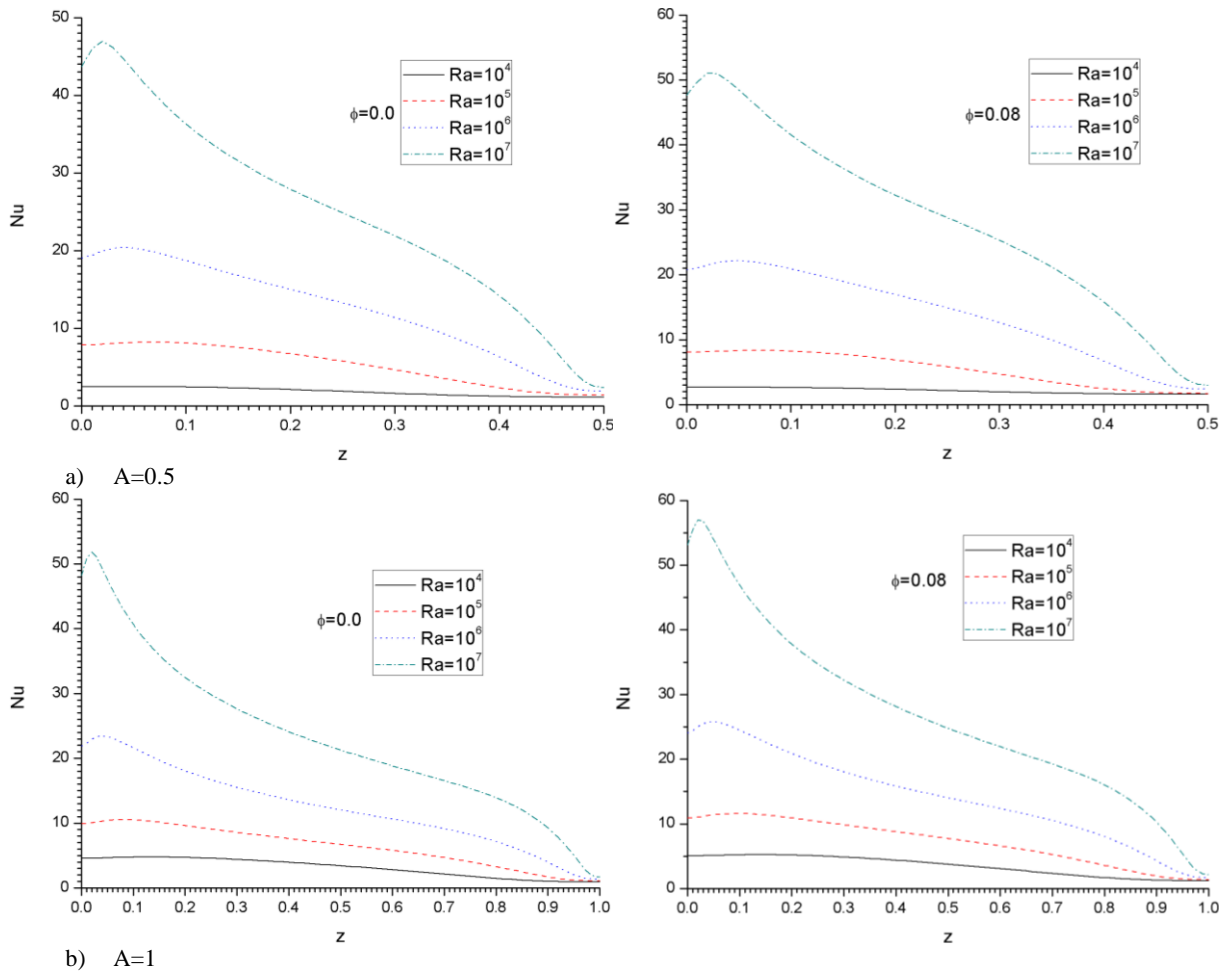


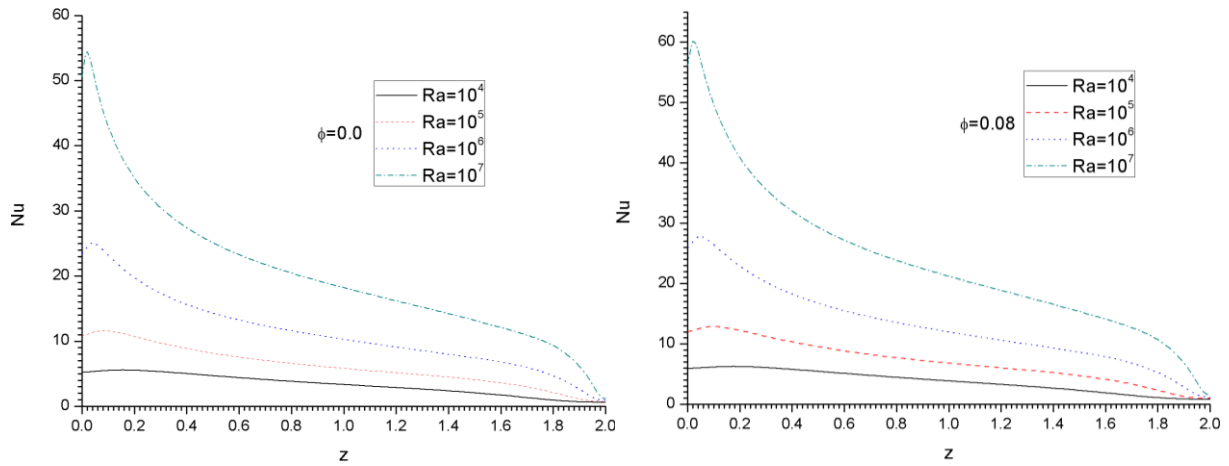
$\phi=0.08$





**Figure 4.** Streamlines (on the left) and isotherms (on the right) for 0:100% EG/W-based nanofluid for  $A=2$  and  $R_o/R_i=2$ .





c)A=2

**Figure 5.** Local Nusselt number of 50:50% EG/W for various values of Rayleigh number, solid volume fraction and aspect ratio ( $R_o/R_i=2$ ).

**Table 4.** Variation of the average Nusselt number for A=0.5 and  $R_o/R_i=2$ .

| Ra     | $\phi$ | 0:100% EG/W | 50:50% EG/W | 100:0% EG/W |
|--------|--------|-------------|-------------|-------------|
| $10^4$ | 0.00   | 1.84        | 1.84        | 1.84        |
|        | 0.04   | 1.98        | 1.98        | 1.98        |
|        | 0.08   | 2.14        | 2.16        | 2.16        |
| $10^5$ | 0.00   | 5.28        | 5.30        | 5.30        |
|        | 0.04   | 5.40        | 5.40        | 5.42        |
|        | 0.08   | 5.44        | 5.44        | 5.50        |
| $10^6$ | 0.00   | 12.44       | 12.46       | 12.48       |
|        | 0.04   | 13.14       | 13.20       | 13.24       |
|        | 0.08   | 13.78       | 13.84       | 13.94       |
| $10^7$ | 0.00   | 24.98       | 25.04       | 25.04       |
|        | 0.04   | 26.68       | 26.80       | 26.88       |
|        | 0.08   | 28.32       | 28.46       | 28.64       |

**Table 6.** Variation of the average Nusselt number for A=2 and  $R_o/R_i=2$ .

| Ra     | $\phi$ | 0:100% EG/W | 50:50% EG/W | 100:0% EG/W |
|--------|--------|-------------|-------------|-------------|
| $10^4$ | 0.00   | 3.29        | 3.30        | 3.30        |
|        | 0.04   | 3.53        | 3.54        | 3.55        |
|        | 0.08   | 3.76        | 3.77        | 3.79        |
| $10^5$ | 0.00   | 6.09        | 6.10        | 6.11        |
|        | 0.04   | 6.54        | 6.57        | 6.59        |
|        | 0.08   | 6.99        | 7.03        | 7.08        |
| $10^6$ | 0.00   | 11.18       | 11.21       | 11.21       |
|        | 0.04   | 12.04       | 12.09       | 12.13       |
|        | 0.08   | 12.89       | 12.97       | 13.05       |
| $10^7$ | 0.00   | 20.25       | 20.32       | 20.33       |
|        | 0.04   | 21.84       | 21.95       | 22.03       |
|        | 0.08   | 23.41       | 23.57       | 23.72       |

**Table 5.** Variation of the average Nusselt number for A=1 and  $R_o/R_i=2$ .

| Ra     | $\phi$ | 0:100% EG/W | 50:50% EG/W | 100:0% EG/W |
|--------|--------|-------------|-------------|-------------|
| $10^4$ | 0.00   | 3.14        | 3.15        | 3.15        |
|        | 0.04   | 3.33        | 3.33        | 3.34        |
|        | 0.08   | 3.50        | 3.50        | 3.53        |
| $10^5$ | 0.00   | 6.40        | 6.41        | 6.41        |
|        | 0.04   | 6.82        | 6.84        | 6.86        |
|        | 0.08   | 7.22        | 7.25        | 7.30        |
| $10^6$ | 0.00   | 12.37       | 12.40       | 12.40       |
|        | 0.04   | 13.26       | 13.30       | 13.35       |
|        | 0.08   | 14.12       | 14.19       | 14.28       |
| $10^7$ | 0.00   | 23.10       | 23.16       | 23.17       |
|        | 0.04   | 24.84       | 24.95       | 25.03       |
|        | 0.08   | 26.55       | 26.70       | 26.87       |

**Table 7.** Variation of the average Nusselt number for A=0.5 (water-based nanofluid).

| Ra     | $\phi$ | $R_o/R_i=2$ | $R_o/R_i=3$ | $R_o/R_i=4$ |
|--------|--------|-------------|-------------|-------------|
| $10^4$ | 0.00   | 1.84        | 2.29        | 2.68        |
|        | 0.04   | 1.98        | 2.46        | 2.90        |
|        | 0.08   | 2.14        | 2.69        | 3.18        |
| $10^5$ | 0.00   | 5.28        | 6.22        | 6.93        |
|        | 0.04   | 5.40        | 6.38        | 7.15        |
|        | 0.08   | 5.44        | 6.48        | 7.31        |
| $10^6$ | 0.00   | 12.44       | 14.24       | 15.48       |
|        | 0.04   | 13.14       | 15.07       | 16.41       |
|        | 0.08   | 13.78       | 15.83       | 17.28       |
| $10^7$ | 0.00   | 24.98       | 28.28       | 30.40       |
|        | 0.04   | 26.68       | 30.22       | 32.51       |
|        | 0.08   | 28.32       | 32.10       | 34.55       |

**Table 8.** Variation of the average Nusselt number for A=1 (water-based nanofluid).

| Ra              | R <sub>o</sub> /R <sub>i</sub> =2 | R <sub>o</sub> /R <sub>i</sub> =3 | R <sub>o</sub> /R <sub>i</sub> =4 | R <sub>o</sub> /R <sub>i</sub> =2 |
|-----------------|-----------------------------------|-----------------------------------|-----------------------------------|-----------------------------------|
| 10 <sup>4</sup> | 0.00                              | 3.14                              | 3.75                              | 4.24                              |
|                 | 0.04                              | 3.33                              | 3.99                              | 4.53                              |
|                 | 0.08                              | 3.50                              | 4.21                              | 4.81                              |
| 10 <sup>5</sup> | 0.00                              | 6.40                              | 7.41                              | 8.16                              |
|                 | 0.04                              | 6.82                              | 7.92                              | 8.74                              |
|                 | 0.08                              | 7.22                              | 8.41                              | 9.31                              |
| 10 <sup>6</sup> | 0.00                              | 12.37                             | 14.10                             | 15.27                             |
|                 | 0.04                              | 13.26                             | 15.13                             | 16.41                             |
|                 | 0.08                              | 14.12                             | 16.13                             | 17.53                             |
| 10 <sup>7</sup> | 0.00                              | 23.10                             | 26.10                             | 28.01                             |
|                 | 0.04                              | 24.84                             | 28.08                             | 30.14                             |
|                 | 0.08                              | 26.55                             | 30.02                             | 32.25                             |

**Table 9.** Variation of the average Nusselt number for A=2 (water-based nanofluid).

| Ra              | φ    | R <sub>o</sub> /R <sub>i</sub> =2 | R <sub>o</sub> /R <sub>i</sub> =3 | R <sub>o</sub> /R <sub>i</sub> =4 |
|-----------------|------|-----------------------------------|-----------------------------------|-----------------------------------|
| 10 <sup>4</sup> | 0.00 | 3.29                              | 3.91                              | 4.41                              |
|                 | 0.04 | 3.53                              | 4.21                              | 4.76                              |
|                 | 0.08 | 3.76                              | 4.49                              | 5.10                              |
| 10 <sup>5</sup> | 0.00 | 6.09                              | 7.06                              | 7.78                              |
|                 | 0.04 | 6.54                              | 7.60                              | 8.40                              |
|                 | 0.08 | 6.99                              | 8.15                              | 9.03                              |
| 10 <sup>6</sup> | 0.00 | 11.18                             | 11.21                             | 11.21                             |
|                 | 0.04 | 12.04                             | 12.09                             | 12.13                             |
|                 | 0.08 | 12.89                             | 12.97                             | 13.05                             |
| 10 <sup>7</sup> | 0.00 | 20.25                             | 22.90                             | 24.60                             |
|                 | 0.04 | 21.84                             | 24.69                             | 26.54                             |
|                 | 0.08 | 23.41                             | 26.48                             | 28.48                             |

## CONCLUSION

The laminar natural convection of Al<sub>2</sub>O<sub>3</sub> nanofluids between two vertical concentric cylinders was investigated in this study for various values of the Rayleigh number, solid volume fraction, ethylene glycol to water volume ratio, aspect ratio, and radius ratio. The concluding remarks are:

The average Nu number experiences a considerable increase with increasing Ra number. The average Nu number is also highly dependent on the radius ratio and increases significantly with an increase in the radius ratio. The effect of the radius ratio is more profound for the low values of Ra number and high values of the solid volume fraction. The average Nu number displays an increase with increasing nanoparticle volume fraction. The increase in the average Nu number with the solid volume fraction is lower for low values of Ra number and radius ratio. The dependence of the average Nusselt number on the volume ratio of EG to water is considerably low. The average Nu number experiences first an increase and then a decrease with an increase in the aspect ratio for the high values of the Ra number.

The average Nu number shows a steady low increase with the aspect ratio for the low values of the Ra number.

## REFERENCES

- Alawi O.A., Sidik N.A.C. and Dawood H.K., 2014, Natural Convection Heat Transfer in Horizontal Concentric Annulus Between Outer Cylinder and Inner Flat Tube using Nanofluid, *Int. Comm. in Heat and Mass Transfer*, 5765–5771.
- Abu-Nada E., Masoud Z. and Hijazi A., 2008, Natural Convection Heat Transfer Enhancement in Horizontal Concentric Annuli using Nanofluids, *Int. Comm. in Heat and Mass Transfer*, 35, 657–665.
- Brinkman, H.C., 1952, The Viscosity of Concentrated Suspensions and Solutions, *J. Chem. Phys.*, 4, 571–581.
- Cabaleiro D, Colla L., Agresti F., Lugo L. and Fedele L. 2015, Transport Properties and Heat Transfer Coefficients of ZnO/(ethylene glycol + water) Nanofluids, *Int. J. of Heat and Mass Transfer*, 89, 433–443.
- Chen W.C., Chen Y.F. and Cheng W.T., 2016, Numerical Simulation on Forced Thermal Flow of Nanofluid in the Gap between Co-axial Cylinders with Rotational inner Spindle, *Int. J. of Heat and Mass Transfer*, 102,971–979.
- Cianfrini M., Corcione M. and Quintino A., 2011, Natural Convection Heat Transfer of Nanofluids in Annular Spaces between Horizontal Concentric Cylinders, *Appl. Thermal Engineering*, 3,14055-4063.
- Davis G. de Vahl and Thomas R. W., 1969, Natural Convection between Concentric Vertical Cylinders, *Physics of Fluids* 12, 198- 207.
- Dawood H.K., Mohammed H.A., Sidik N.A.C., Munisamy K.M. and Alawi O.A., 2017, Heat Transfer Augmentation in Concentric Elliptic Annular by Ethyleneglycol Based Nanofluids, *Int. Comm. in Heat and Mass Transfer*, 82, 29–39.
- Fuchs, L. and Eguchi, Y. 1988, On the Accuracy of Finite-Difference and Finite-Element Methods for the Simulation of Some Incompressible Flows. *Computational Mechanics* 4, 105–114.
- Haq R.U., Shahzad F Al-Mdallal. and Q.M., 2017, MHD Pulsatile Flow of Engine Oil Based Carbon Nanotubes Between Two Concentric Cylinders, *Results in Physics*, 7, 57–68.
- Hajmohammadi M.R., 2017, Cylindrical Couette Flow and Heat Transfer Properties of Nanofluids; Single-Phase and Two-Phase Analyses, *J. of Molecular Liquids*, 240, 45–55.

Heris S.Z., Shokrgozar M., Poorpharhang S., Shanbedi M. and Noie S.H., 2014, Experimental Study of Heat Transfer of a Car Radiator with CuO/Ethylene Glycol-Water as a Coolant, *J. Disper. Sci. Technol.*, 35, 677–684.

Hinge H., Chaudhri P. E., Barhate S. H. and Dhokane N. 2017, Boiling Heat Transfer Enhancement of Heat Pipe Using Nanofluid, *Int. Journal of Curr. Engineering and Technol.*, 7, 244-251.

Jiajan W., 2010, *Solution to Incompressible Navier Stokes Equations by using Finite Element Method*, Ms Thesis, The University of Texas at Arlington, USA.

Keblinski P., Phillpot SR, Choi S.U.S. and Eastman J.A., 2002, Mechanisms of Heat Flow in Suspensions of Nano-Sized Particles (Nanofluids), *Int. J. Heat Mass Transfer* 45, 855–863.

Maghlany W.M.E. and Elazm M.M.A., 2016, Influence of Nanoparticles on Mixed Convection Heat Transfer in an Eccentric Horizontal Annulus with Rotating Inner Cylinder, *J. of the Taiwan Institute of Chemical Engineers*, 63,259–270.

Mitra S.K, Chakraborty S., 2011, *Microfluidics and Nanofluidics Handbook*, 2 Volume Set 1st Edition, CRC Press Published, September 20.

Özdemir K. and Ögüt E. 2019, Hydro-Thermal Behaviour Determination and Optimization of Fully Developed Turbulent Flow in Horizontal Concentric Annulus with Ethylene Glycol and Water Mixture Based Al<sub>2</sub>O<sub>3</sub> Nanofluids, *Int. Comm. in Heat and Mass Transfer*, 109,1-13.

Öztuna S., Kahveci K. and Tanju B.T., 2011, Natural Convection of Water-Based CuO Nanofluid Between Concentric Cylinders, *Recent Advances in Fluid Mechanics and Heat & Mass Transfer, Florence, Italy*, 164-169.

Said Z., Sajid M.H., Alim M.A., Saidur R. and Rahim N.A., 2013, Experimental Investigation of The Thermophysical Properties of Al<sub>2</sub>O<sub>3</sub>-Nanofluid and its Effect on a Flat Plate Solar Collector, *Int. Comm. in Heat and Mass Transfer*, 48, 99–107.

Sasmal C., 2017, Effects of Axis Ratio, Nanoparticle Volume Fraction and its size on The Momentum and Heat Transfer Phenomena from an Elliptic Cylinder in Water-Based CuO Nanofluids, *Powder Technology*, 313, 272–286.

Selimefendigil F. and Öztop H.F., 2017, Conjugate Natural Convection in Nanofluid Filled Partitioned Horizontal Annulus Formed by Two Isothermal Cylinder Surfaces under Magnetic Field, *Int. J. of Heat and Mass Transfer*, 108, 156–171.

Srinivasacharya D. and Shafeurrahman Md., 2017, Hall and Ion Slip Effects On Mixed Convection Flow of Nanofluid Between Two Concentric Cylinders, *J. of the Association of Arab Universities for Basic and Applied Sciences*, 24, 223–230.

Togun H., Abu-Mulaweh H.I., Kazi S.N. and Badarudin A., 2016, Numerical Simulation of Heat Transfer and Separation Al<sub>2</sub>O<sub>3</sub>/Nanofluid Flow in Concentric Annular Pipe, *Int. Comm. in Heat and Mass Transfer*, 71, 108–117.

Turkyilmazoglu M., 2015, Anomalous Heat Transfer Enhancement by Slip Due To Nanofluids in Circular Concentric Pipes, *Int. J. of Heat and Mass Transfer* 85, 609–614.

Wu W., Zhou Z., Aubry N., Antaki J.F. and Massoudi M., 2017, Heat Transfer and Flow of a Dense Suspension Between Two Cylinders, *Int. J. of Heat and Mass Transfer*, 112, 597–606.

Xuan, Y. and Roetzel, W., 2000, Conceptions for Heat Transfer Correlation of Nanofluids, *Int. J. Heat Mass Transfer*, 43,3701–3707.

Yu W. and Choi S.U.S., 2003, The Role of Interfacial Layer in The Enhanced Thermal Conductivity of Nanofluids: a Renovated Maxwell Model, *J Nanoparticles Res.*, 5, 167–171.

Yu Z., Xu X., Hu Y., Fan L. and Cen K., 2012, A Numerical Investigation of Transient Natural Convection Heat Transfer of Aqueous Nanofluids in a Horizontal Concentric Annulus, *Int. J. of Heat and Mass Transfer*, 55, 1141–1148.



**Kamil KAHVECİ** graduated from Trakya University with a BS and PhD degree in Mechanical Engineering. He is currently working as a Professor in the Mechanical Engineering Department at Trakya University. His research interests include Computational Fluid Dynamics, Convective Heat Transfer and Mass Transfer in Porous Media.



**Elif Büyük ÖĞÜT** graduated from Trakya University with a BS and PhD in Mechanical Engineering. She is currently a Professor in the Vocational School of Hereke at Kocaeli University. Her research interests include Computational Fluid Dynamic, MHD, Natural and Mixed Convection in Enclosure and Heat Transfer in Nanofluids.